2019 IEEE PES/IAS PowerAfrica

Eddy current losses computation in conductives materials: case of Aluminum and Permanent Magnet-Part I: Frequency and current effects

P. K. Chetangny, J. G. Aredjodoun, S. Houndedako, A. Vianou
Polytechnic School of Abomey-Calavi
University of Abomey-Calavi
Abomey-Calavi, Benin
chetangny@yahoo.com

D. Chamagne
Energy Department
FEMTO-ST - UMR CNRS 6174
University of Bourgogne Franche-Comte
Belfort, France
didier.chamagne@univ-fcomte.fr

G. Barbier
Laboratoire de Physique et Mécanique Textiles (LPMT)
Université de Haute Alsace
(UHA - ENSISA)
Mulhouse, France
gerald.barbier@uha.fr

***Abstract*—This paper presents a method for calculation of eddy current losses in the conductive material such as permanent magnet and aluminum. A quasi-3D analytical model is developed and the results have been compared to an experimental test. A U-cored Electromagnet Device is used to evaluate eddy current losses generated in the conductive material. The analytical method considers only the effect of frequency, current for differents thickness of the conductives materials. The novelty of this work is based on the modeling by electrical equivalent circuit to find the boundary conditions needed and to verify the assumptions made on the current density by FE results, when solving the Maxwell equations.**

Keywords— Aluminum, analytical model, eddy current losses, experimental test, permanent magnet

I. INTRODUCTION

A. Scientific Context

The work presented in this paper is a part of various research programs on the modeling and design of synchronous machines with permanent magnets, for land transport applications. Indeed, the current trend, whether in rail traction, or in electric vehicles and / or electric hybrids, is to use such engines for their high mass performance and good performance. This trend can also be seen in large direct attack wind turbines. However, a disadvantage of these machines is the existence of losses that can be significant in permanent magnets. Although these losses do not significantly reduce the machine efficiency or performance, they may result in a temperature rise inside the magnets which can cause partial or total irreversible demagnetization [1],[2],[3]. In this context, the objective of this work is to establish new models, more accurate, of eddy current losses in conductives materials such as permanents magnets and aluminum. In the literature the eddy currents losses in conductive materials (e.g. rare-earth permanent magnets, Aluminum ...) in electric machines, are difficult to determine. They represent in recent years, a significant part of the scientific research in electrical engineering. So many models both analytical and numerical exist but they are mostly in 2D and does not take into account the 3D distribution of eddy currents. In [4] an experimental device is used for measuring the eddy current losses. In this paper, the experimental results obtained from the test device are used and have been compared to those obtained from the analytical model.

B. Review of litterature

In recent years the calculation of the losses induced in the permanents magnets has led to major research work in the field of modeling of electric actuators. There are different models and methods for calculating these losses induced by eddy currents, not only in the magnets, but also in all conductive materials such as aluminum for example. Among the various models proposed, we have 2D analytical ones based on the resolution of the Maxwell equations while taking into account the magnetic reaction of armature in the magnets [5] or those with limited resistance [6], [7]. The first leads to the analytical resolution of the diffusion equation in the magnets; this is the case of [8] where the authors used the subdomain method. Other simple models based on the flux calculation created by the magnetic induction variation, assume that eddy currents flow in the conductive material as a loop [9], [10], [11]. In [12] a simple model of the magnet which approximates the distribution of the current by an equivalent way, because the effect of skin is neglected. Another approach for calculating losses in the case of permanent magnet synchronous machine, proposed by several authors [6],[13] and [14], consists in replacing the currents flowing in the stator windings by a uniform linear current density along the stator slots. The total losses are obtained by summing those due to the different frequencies of the temporal and spatial harmonics. Most of the approaches presented above neglect the 3D effects of currents induced with the assumption of a very large axial dimension of the magnet compared to the others dimension. However, this assumption is not always valid and 2D approaches can introduce significant errors in the calculation of induced current losses. To account for the 3D effects of the induced currents [15] introduces a correction factor which must be, for the case of a Permanent magnet synchronous machines, calculated for each harmonic of the magnetomotive force. The approaches presented above do not take into account the effect of skin. Under certain circumstances, since the permeability of the conductive material is small, the thickness of the skin can become very large compared to the width of the conductive material and significant errors can occur neglecting this effect as shown in [16]. The author proposed two methods to take into account this effect: a global approach of energy and an approach using the Fourier series decomposition of the magnetomotive force, the last approach being more precise. In both cases, in addition to the skin effect, end effects are also taken into account by a coefficient.

978-1-7281-1010-3/19/$31.00 ©2019 IEEE

II. MEASUREMENT SYSTEM AND ELECTRICAL EQUIVALENT CIRCUIT

The experimental device we used in this work is a flat armature presented in Fig. 1 because we already have in the laboratory this type of electromagnet. However a task no less important is the characterization of this device wich in made in [4]. Table I present the main dimensions of the test device.

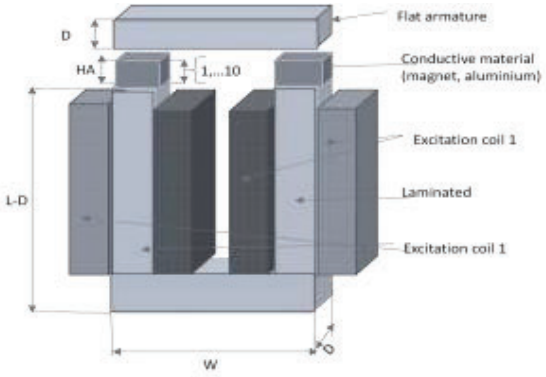

Fig. 1. Schematic representation of the experimental device

TABLE I. main dimensions of test device

Symbol	QUANTITY	Value
L	Length	190 mm
W	width	150mm
D	Deep	43mm
HA	Material width	1 to 10 mm
A	Cross section	43x43 mm2

The test device is composed of a magnetic circuit made of high performance electrical steel of 0.5 mm thickness. The cross section is 43mm x43 mm and the weight is about 7.5 kg. The device is subject to an alternating field created by two identical excitation coils '(each with 500 turns) connected in parallel. The air-gap with, the supply frequency and the flux density can be varied.

III. QUASI 3D ANALYTICAL CALCULATIONS BASED ON MAXWELL EQUATIONS

Eddy currents are among the effects that occur in regions when operating in steady-state conditions. In other words, the displacement currents inside the conductive materials can always be neglected with respect to the current in the conductor. This is true even for materials with very high electrical conductivities. Eddy currents cause a nonuniform distribution of the current density in a considered section of conductive material. This naturally results in an increase in

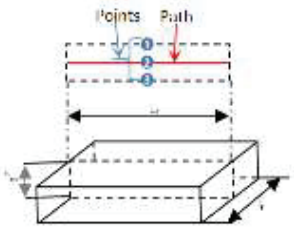

Fig. 2. Material in 3D with points and path [4]

Joule losses. These eddy currents and the nonuniform distribution of associated magnetic flux give rise to phenomena such as the skin effect. An increase in the current density causes an increase in the effective resistance of a conductor with respect to the DC resistance and also a decrease in the inductance [17]. To model a problem of skin or eddy current effects, we start from the Maxwell equations that we modify for the quasi-stationary regime. In [18], problems concerning magnetic fields and current flows are often formulated in terms of differential or integral equations. Differential equations describe the fate of the magnetic field or bound quantities at a point in terms of local source of current density. These equations are then solved in a given region and the influences of the sources outside the region are taken into account in the solution thanks to the boundary conditions. Integral equations on the other hand express the field taking from all sources (the effects of all sources being summed to give the resulting field). It may seem more efficient to solve Maxwell's equations rather than using differential equations, but in fact integral equations are usually more difficult to solve. By omitting the displacement currents, which are negligible in quasi- stationary conductors, the basic equations of the field are:

$$rotE = -\frac{\partial B}{\partial t} \tag{1}$$

$$rotH = J \tag{2}$$

$$divB = 0 \tag{3}$$

Where B represent the flux density, H the magnetic field and J the current density. For a linear materialor or a material with constant conductivity, we found : by combining Maxwell Faraday (1), Maxwell Ampere (2) and equation (3):

$$\nabla^2 H = \sigma\mu_0\mu_r \frac{\partial H}{\partial t} \tag{4}$$

With these equations, several possibilities of resolutions are offered and it is possible to make a resolution in 2D [17] and then to extend it in 3D. Let the current flow in the y direction only and Jy, Hx and Hz are function of x and z or let the magnetic field have a single component in the y direction and Hy, Jx and Jz are function of x and z. In the first case, it is wiser to use the vector potential that is parallel to the current density in y direction On the other side the magnetic field has two components.

In Cartesian coordinates (8) can also be written

$$\frac{\partial^2 H}{\partial x^2} + \frac{\partial^2 H}{\partial y^2} + \frac{\partial^2 H}{\partial z^2} = \sigma\mu \frac{\partial H}{\partial t} \tag{5}$$

The quasi 3D method is used in Cartesian coordinates for solving the magnetic field equations, where the following assumptions are considered:

1. Only normal component(y) of magnetic flux density (B) to magnet surface is considered.
2. Normal component component (y) of current density (J) to magnet surface is considered zero.

To verify these assumptions we use FE simulation with Flux 3D and we plot at diffrents points and on a path (Fig.2) in the material, the current density as shown in Fig.3.

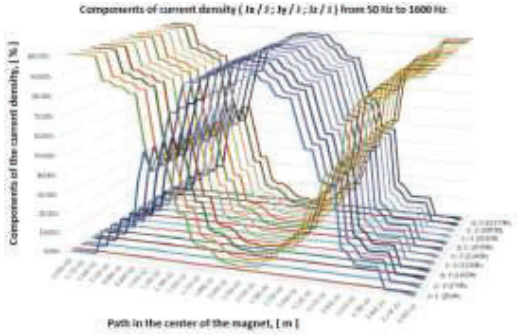

Fig. 3. Current density components from 50Hz to 1.6 kHz

We can notice in Fig.3 that the percentage of the second component (Jy) of the current density is insignificant compared to module of J. This confirm that we can neglect the components (Hx and Hz) of the field or the flux density.

The differential equation with the single component of the magnetic field Hy inside the conductor of constant conductivity, can be obtained from the equation (5) according to Fig.3 and by using complex formulation becomes:

$$\frac{\partial^2 \underline{H}_y}{\partial x^2} + \frac{\partial^2 \underline{H}_y}{\partial z^2} = \alpha^2 \frac{\partial \underline{H}_y}{\partial t} \tag{6}$$

Where $\alpha^2 = \sigma \mu_0 \mu_r jw$

Using the method of variable separation allows us to solve the partial differential equation (6).

$$\underline{H}_y(x,z) = \sum_{m=0}^{\infty} \left[\begin{Bmatrix} \{K_{\Gamma m} \sin(\Gamma m x) + L_{\Gamma m} \cos(\Gamma m x)\} \\ \times \begin{Bmatrix} M_{\Gamma m} \sinh(\sqrt{\alpha^2 + \Gamma m^2}\, z) \\ + N_{\Gamma m} \cosh(\sqrt{\alpha^2 + \Gamma m^2}\, z) \end{Bmatrix} \end{Bmatrix} + \sum_{n=0}^{\infty} \left[\begin{Bmatrix} \{P_{\zeta n} \sin(\zeta n z) + Q_{\zeta n} \cos(\zeta n z)\} \\ \times \begin{Bmatrix} R_{\zeta n} \sinh(\sqrt{\alpha^2 + \zeta n^2}\, x) \\ + S_{\zeta n} \cosh(\sqrt{\alpha^2 + \zeta n^2}\, x) \end{Bmatrix} \end{Bmatrix} \tag{7}$$

With $K_{\Gamma m}$, $M_{\Gamma m}$, $N_{\Gamma m}$, $P_{\zeta n}$, $R_{\zeta n}$ and $S_{\zeta n}$ the separation constants and coefficients to be determined by the boundary conditions. By applying boundary conditions shown on Fig.4 where the magnetic field applied on the boundary is found by using a network reluctance and considering that Hy is the only component of the magnetic field. It is necessary to specify both Hy and ∂Hy/∂n at the limits, where n is the normal to the boundary surface. This problem involving at least two interconnected regions, it is necessary to use the conditions of continuity at the interfaces: the first condition being that the normal component of the flux density, is continuous that is to say Bn1 = Bn2; the second being that the discontinuity of the tangential component of the magnetic field is equal to the surface density of current, that is to say Ht2 - Ht1 = cste.

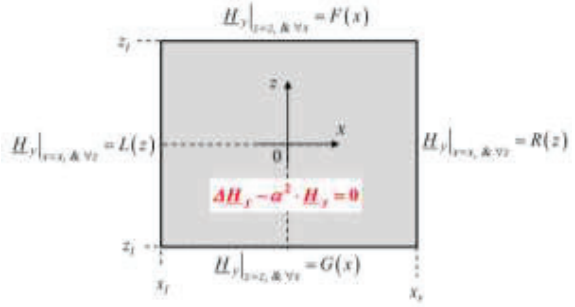

Fig. 4. Boundary conditions

By applying theses conditions, the final solution of eddy current density is given by:

$$rot \underline{H}_y = \underline{J} \tag{8}$$

Where

$$\underline{H}_y(x,z,\theta) = \underline{H}_{y_{\max}}(x,z) e^{j\theta} \tag{9}$$

The current density is given by equations (10) and (11)

$$J_{x_{\max}}(x,z) = -H_s \left[\alpha \frac{\sinh(\alpha z)}{\sinh(\alpha b)} - \sum_n Q_n \sin(\zeta_n z) \frac{\cosh(\sqrt{\alpha^2 + \zeta_n^2}\, x)}{\cosh(\sqrt{\alpha^2 + \zeta_n^2}\, a)} \right] \tag{10}$$

$$J_{z_{\max}}(x,z) = H_s \sum_n Q_n \sqrt{\alpha^2 + \zeta_n^2} \cos(\zeta_n z) \frac{\sinh(\sqrt{\alpha^2 + \zeta_n^2}\, x)}{\cosh(\sqrt{\alpha^2 + \zeta_n^2}\, a)} \tag{11}$$

where

$J_{x_{\max}}(x,z,\theta) = J_{x_{\max}}(x,z) e^{j\theta}$ et $J_{z_{\max}}(x,z,\theta) = J_{z_{\max}}(x,z) e^{j\theta}$

The vector of instantaneous power density in W / m2, called Poynting vector, is define by the vector product:

$$S(r,t) = E(r,t) \wedge H(r,t) \tag{12}$$

In sinusoidal steady state, the complex vector of Poynting is written:

$$S(r) = \frac{1}{2} \underline{E}(r,t) \wedge \underline{H}^*(r,t) \tag{13}$$

To calculate the losses in the material, we used the Poynting vector which represents the energy flow density. In other words, the electromagnetic power P which passes through a surface S is the flow of the Poynting vector through this surface.

$$\underline{E}(r) = \frac{1}{\sigma} \underline{J}(r) \tag{14}$$

We can also whrite

$$S(r)=\frac{1}{2}\frac{1}{\sigma}\underline{J}(r)\wedge\underline{H}^{*}(r,t) \tag{15}$$

By applying Poynting's theorem in our case where

$$\underline{J}=\begin{pmatrix}\underline{J}_x\\0\\\underline{J}_z\end{pmatrix}\text{ and }\underline{H}=\begin{pmatrix}0\\\underline{H}_y\\0\end{pmatrix} \tag{16}$$

and we obtain:

$$\underline{J}\wedge\underline{H}^{*}=\begin{pmatrix}-\underline{J}_z.\underline{H}_y^{*}\\0\\\underline{J}_x.\underline{H}_y^{*}\end{pmatrix}\text{ and }ds=\begin{pmatrix}dydz\\dxdz\\dxdy\end{pmatrix} \tag{17}$$

Eddy current losses are calculated by using poynting theorem:

$$S(r,t)=E(r,t)\wedge H(r,t) \tag{18}$$

Where S(r,t) is the power density vector in W/m^2

The average active power is then given by :

$$P=\frac{1}{2}\frac{1}{\sigma}\oiint\mathrm{Re}\left[\left(\underline{J}.\underline{H}^{*}\right)ds\right] \tag{19}$$

or

$$P=\frac{1}{2}\frac{1}{\sigma}\oiint\mathrm{Re}\left[-\underline{J}_x.\underline{H}_y^{*}dx+\underline{J}_z.\underline{H}_y^{*}dz\right] \tag{20}$$

After simplification the eddy current losses is given by:

$$P=\frac{1}{2}\frac{1}{\sigma}\cdot hm\int\mathrm{Re}\begin{bmatrix}(\underline{J}_x\cdot\underline{H}_y^{*}\cdot dx\\-\underline{J}_z\cdot\underline{H}_y^{*}\cdot dz\end{bmatrix} \tag{21}$$

IV. Effect of Frequency on the Losses

The evolution of eddy current losses varies according to the material. For alumina we could say that these losses vary according to the scare root of the frequency f while they vary according to the square of the frequency f for the magnet as shown in Figures 5 and 6.

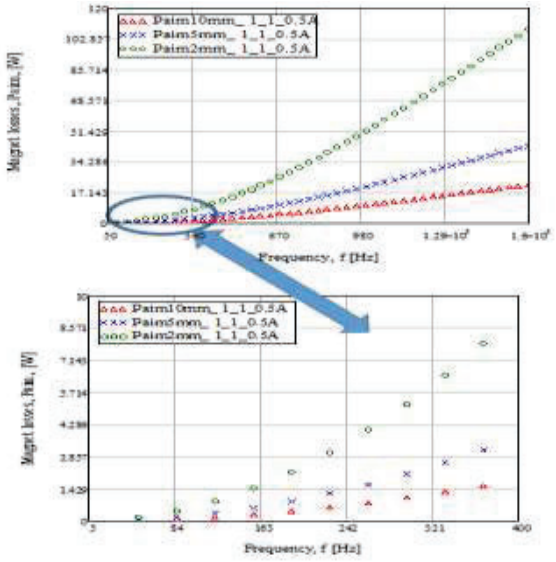

Fig. 5. Eddy current losses in function of frequency in the magnet for different material thicknesses

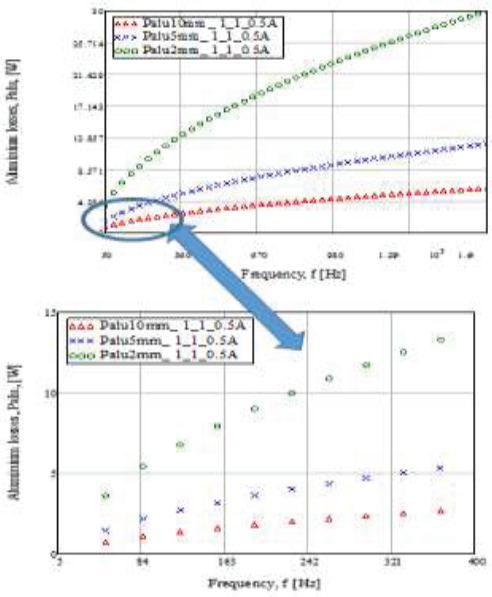

Fig. 6. Eddy current losses in function of frequency in the Aluminum for different material thicknesses

V. Effect of Current and Thickness on the Losses

Figures 7 and 8 shows the losses induced in aluminum and in magnet for different thicknesses at 50 Hz and at 1600 Hz a quadratic depending on the current in both low and high frequency, for both materials. Moreover, for three pieces of the same section and of different thicknesses, the losses decrease with the increase of the thickness for the same given current.

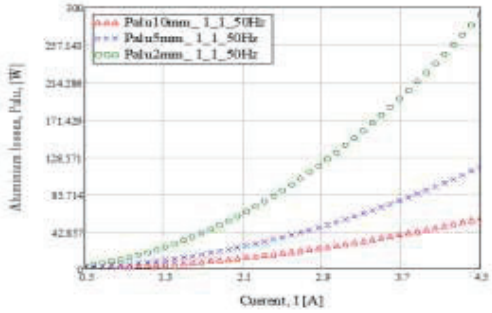

(a)

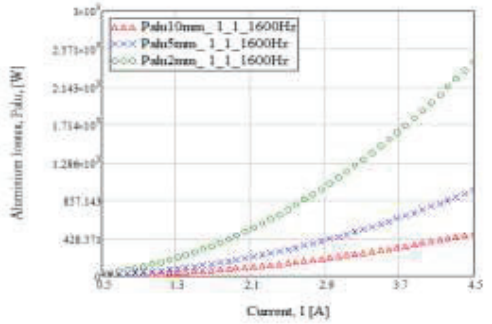

(b)

Fig. 7. Aluminum losses in function of frequency (a) at 50 Hz and (b) at 1.6 kHz

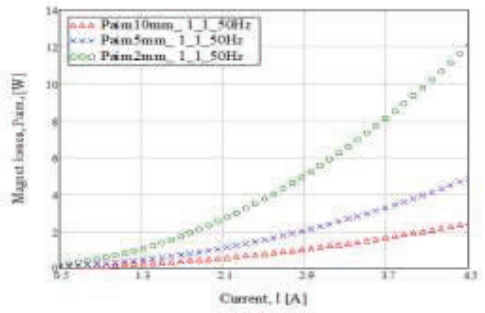

(a)

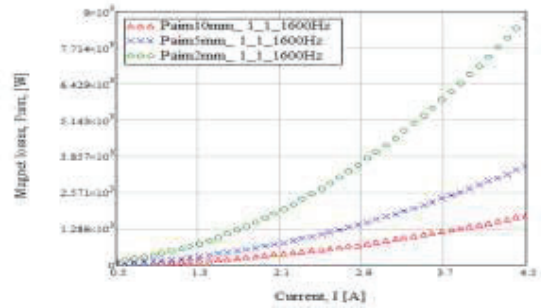

(b)

Fig. 8. Magnet losses in function of current (a) at 50 Hz and (b) at 1.6 kHz

VI. Comparison of Analytical and Experimental Results

At 50 Hz and low frequency, the difference between the experimental results and the analytical model is negligible. Experimental values are slightly higher than the results obtained of the analytical model. This difference is smaller for massive pieces of 2 mm than for those of 5 mm and 10 mm. Beyond 100 Hz the difference widens more but remains nevertheless weak. This can be explained by both the skin effect and the hypotheses of the analytical calculus. Beyond 200 Hz and for 1.6kHz, the skin effect becomes more precise as are the leaks that become more important. The figures below show a comparison of evolution losses measured and calculated as a function of the current for different frequencies.

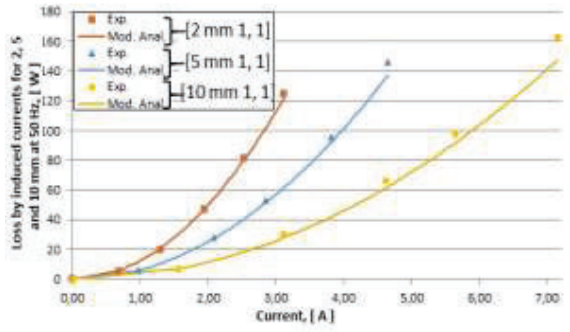

(a)

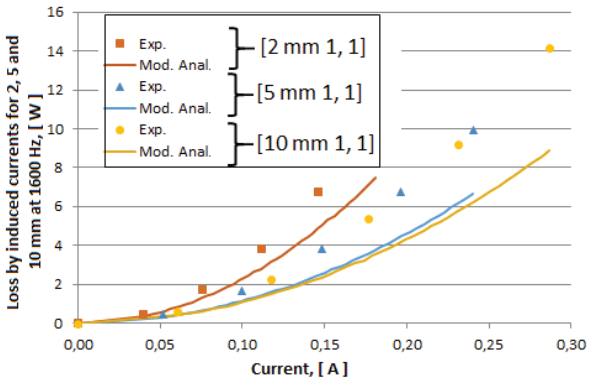

(b)

Fig. 9. Analytical and experimental results at (a) 50 Hz and (b) 1.6 kHz

There is a gap between the experimental results and those obtained from the analytical model. To better understand how this gap evolves we have calculated the proportionality coefficients between the results from the analytical model and those measured. This was possible by linearizing the curves and thus plotting them according to the square of the current. Then by calculating the ratios of the directional coefficients of the lines obtained, we find the different coefficients of proportionality for the different thicknesses of the massive parts used and for the different measurement frequencies. These calculations were made only for configurations that correspond to unsegmented materials. Figures 10 (a) and (b) shows the evolution of these coefficients of proportionality which also reflect the error rate between the measurements and the experimental one. Note that this ratio decreases as the frequency increases. This can be explained by the assumptions made in solving the Maxwell equations, including boundary conditions, determination of the magnetic field applied to the edges and failure to take into account the magnetic reaction of armature.

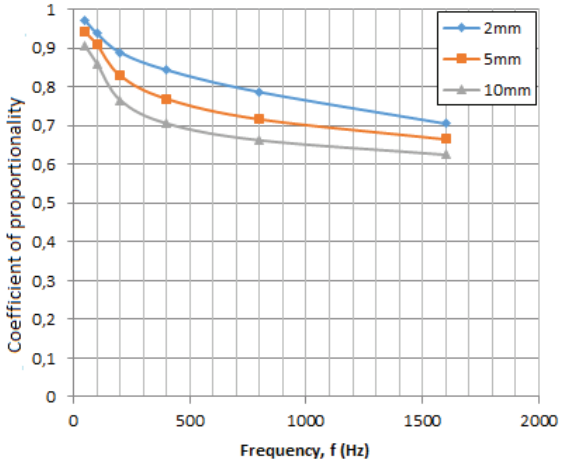

(a)

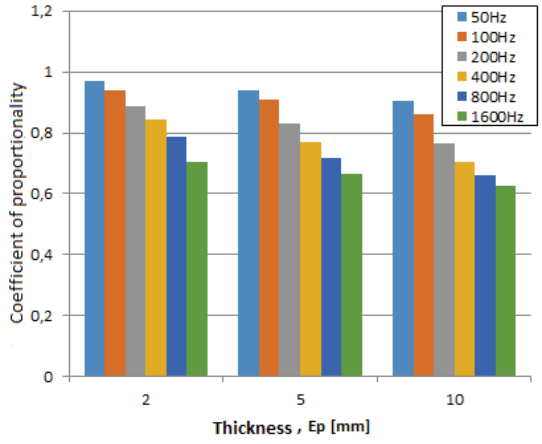

(b)

Fig. 10. Coefficient of proportionality between analytical and experimental results (a) differents frequency and (b) differents thickness

VII. Conclusion

In this paper, we propose to calculate the magnetic losses created by the eddy currents in the conductive materials. To better understand the different physical phenomena involved in the losses for conductives materials, we studied a U-shaped electromagnet with a flat amature, into which conductive materials are inserted. This device allows us to approach in a pragmatic way the problem of the losses in the conductive materials. One of the problems was the separation of these losses from the other losses that occur in the device. Indeed, it is not easy to find the ratio iron loss / material loss since both occur simultaneously in the device and evolve differently in function of frequency. By solving Maxwell equations, we find an analytical model with wich we can estimate the eddy current losses in the conductives materials. We were able to study separately the different effects of the frequency and the current on the losses. The Quasi 3D modeling allows us to analyze the phenomena in a case very close to the real case. By comparing the results obtained analytically and experimentaly we find some acuracy for low frequencies up to a certain value but the results diverge for higher frequencies. This means that some of the assumptions made during the calculation including the Foucault current path, the absence of leaks, the existence of the skin effect, the variation of the magnetic induction in the materials and taking into account the magnetic reaction of armature are important in the calculation of the magnetic field.

References

[1] Y. Katsumi Yamazaki , Member , IEEE , Shunji Ohki , Akira Nezu , Takeshi Ikemi , Kanou, Y. Fukushima, C. Engineering, and E. V Powertrain, "Reduction of Magnet Eddy Current Loss in Interior Permanent Magnet Motors with Concentrated Windings," pp. 3963–3969, 2009.

[2] A. Belahcen and A. Arkkio, "Permanent magnets models and losses in 2D FEM simulation of electrical machines," in *19th International Conference on Electrical Machines, ICEM 2010*, 2010, pp. 1–6.

[3] A. Bettayeb, X. Jannot, and J.-C. Vannier, "Analytical calculation of rotor magnet eddy-current losses for high speed IPMSM," *XIX Int. Conf. Electr. Mach. - ICEM 2010*, pp. 1–6, Sep. 2010.

[4] P. K. Chetangny, S. Houndedako, A. Vianou, and C. Espanet, "Eddy-Current Loss in a Conductive Material Inserted into a U-Cored Electromagnet Device," *2017 IEEE Veh. Power Propuls. Conf. VPPC 2017 - Proc.*, vol. 2018-Janua, pp. 1–6, 2018.

[5] F. Deng, "Commutation-caused eddy-current losses in permanent-magnet brushless DC motors," *IEEE Trans. Magn.*, vol. 33, no. 5, pp. 4310–4318, 1997.

[6] D. Ishak, Z. Q. Zhu, and D. Howe, "Eddy-Current Loss in the Rotor Magnets of Permanent-Magnet Brushless Machines Having a Fractional Number of Slots Per Pole," *2462 IEEE Trans. Magn.*, vol. 41, no. 9, pp. 2462–2469, 2005.

[7] J. Wang, K. Atallah, R. Chin, W. M. Arshad, and H. Lendenmann, "Rotor eddy-current loss in permanent-magnet brushless AC machines," *IEEE Trans. Magn.*, vol. 46, no. 7, pp. 2701–2707, 2010.

[8] F. Dubas and A. Rahideh, "Two-Dimensional Analytical Permanent-Magnet Eddy-Current Loss Calculations in Slotless PMSM Equipped With Surface-Inset Magnets," *IEEE Trans. Magn.*, vol. 50, no. 3, 2014.

[9] W.-Y. Huang, A. Bettayeb, R. Kaczmarek, and J.-C. Vannier, "Optimization of Magnet Segmentation for Reduction of Eddy-Current Losse in Permanent Magnet Synchronous Machine," *IEEE Trans. energy Convers.*, vol. 25, no. 2, pp. 381–387, 2010.

[10] J. Pyrhonen, H. Jussila, Y. Alexandrova, P. Rafajdus, and J. Nerg, "Harmonic loss calculation in rotor surface permanent magnets-new analytic approach," *IEEE Trans. Magn.*, vol. 48, no. 8, pp. 2358–2366, 2012.

[11] B. Aslan, E. Semail, and J. Legranger, "Analytical model of magnet eddy-current volume losses in multi-phase PM machines with concentrated winding," *2012 IEEE Energy Convers. Congr. Expo.*, vol. L, no. 1, pp. 3371–3378, Sep. 2012.

[12] J. Klötzl, M. Pyc, and D. Gerling, "Permanent Magnet Loss Reduction in PM- Machines using Analytical and FEM Calculation," *Ieee*, pp. 98–100, 2010.

[13] K. Atallah, R. Chin, W. M. Arshad, and H. Lendenmann, "Rotor Eddy-Current Loss in Permanent-Magnet Brushless AC Machines," *IEEE Trans. Magn.*, vol. 46, no. 7, pp. 2701–2707, Jul. 2010.

[14] X. Ding and C. Mi, "Modeling of eddy current loss in the magnets of permanent magnet machines for hybrid and electric vehicle traction applications," *2009 IEEE Veh. Power Propuls. Conf.*, no. 1, pp. 419–424, Sep. 2009.

[15] . Wang, F. Papini, R. Chin, W. M. Arshad, and H. Lendenmann, "Computationally efficient approaches for evaluation of rotor eddy current loss in permanent magnet brushless machines," *2009 Int. Conf. Electr. Mach. Syst.*, no. 1, pp. 1–6, Nov. 2009.

[16] F. Martin, "Contribution au dimensionnement optimal de machines synchrones à aimants déposés en surface pour applications à hautes vitesses," 2013.

[17] M. S. Jiri Lammeraner, *Eddy currents - Jiri Lammeraner, Milos Stafl - Google Livres*. 1966.

[18] R. L. Stoll, *The analysis of eddy currents*. Clarendon Press, 1974.